

Chapter 27

The Spatial, Temporal, and Interpretive Limits of Functional MRI

Peter A. Bandettini, Ph.D.

(Written for: Neuropsychopharmacology: The Fifth Generation of Progress)

Unit on Functional Imaging Methods

Laboratory of Brain and Cognition

National Institute of Mental Health

Building 10, Room 1D80

10 Center Dr. MSC 1148

Bethesda, MD 20892-1148

phone: 301-402-1333

fax: 301-402-1370

email: bandettini@nih.gov

Contents

27.1 Introduction

27.2 Contrast in FMRI

27.2.1 Blood Volume

27.2.2 Blood Oxygenation

27.2.3 Blood Perfusion

27.2.4 Hemodynamic Specificity

27.2.5 CMRO

27.3 The Hemodynamic Transfer Function

27.3.1 Location

27.3.2 Latency

27.3.3 Magnitude

27.3.4 Linearity

27.4 Scanner Related Issues

27.4.1 Acquisition Rate

27.4.2 Spatial Resolution

27.4.3 Signal to Noise

27.4.4 Stability

27.4.5 Image quality

27.5 Best Results So Far.

27.5.1 Temporal Resolution

27.5.2 Spatial Resolution

27.6 Neuronal Activation Input Strategies

27.6.1 Block Design

27.6.2 Phase and Frequency Encoding

27.6.3 Orthogonal Designs

27.6.4 Parametric Designs

27.6.5 Event-Related Designs

27.6.6 Free Behavior Designs

27.7 Conclusion

Figure Captions

References

27.1 Introduction

Since its inception in 1991, functional MRI (fMRI) has experienced an explosive growth in the number of users accompanied by steady widening of its range of applications. A recent search of the National Library of Medicine database for articles with “fMRI” or “BOLD” in the title revealed over 1000 citations. Improvements continue in pulse sequence design, data processing, data interpretation, and in the tailoring of cognitive paradigms to the technique’s unique advantages and limits. This chapter describes these receding limits. Specifically, the limits of spatial resolution, temporal resolution, interpretability, and implementation will be discussed. The goal here is to give the reader a perspective of the evolution of fMRI in the past 9 years and a sense of excitement as to its ultimate potential.

A user of fMRI primarily is interested in extracting at least one of three types of neuronal information: Where it is neuronal activity happening, when it is happening, and to what degree is it happening. To optimally extract this information, an understanding of the basics to some of the more esoteric details is necessary. In this chapter, these are presented. First, the basics of fMRI contrast are discussed. Second, the key of fMRI interpretation: the “neuronal-hemodynamic transfer function” is described. Third, an overview of methods by which neuronal activation is played out in fMRI subjects and subsequently measured is given. In this section, the popular technique of “event-related fMRI” (ER-fMRI) is described in detail, along with emerging methods for neuronal information extraction. Fourth, the issues of temporal and spatial resolution are discussed. Fifth, a discussion of the limits of interpretation and potential for further neuronal-

hemodynamic information extraction is carried out. Lastly, some implementation limits of are finally given as a practical guideline.

27.2 Contrast in fMRI

Several types of physiologic information can be mapped using fMRI. This information includes baseline cerebral blood volume(1-3), changes in blood volume (4), baseline and changes in cerebral perfusion (5-10), and changes in blood oxygenation (11-17). Recent advances in fMRI pulse sequence and experimental manipulation have allowed quantitative measures of CMRO₂ changes and dynamic non-invasive measures in blood volume with activation to be extracted fMRI data (18-20).

27.2.1 Blood Volume

In the late 1980's, the use of rapid MRI allowed tracking of transient signal intensity changes over time. One application of this utility was to follow the T2* or T2 - weighted signal intensity as a bolus of an intravascular paramagnetic contrast agent passed through the tissue of interest (2). As it passes through, susceptibility-related dephasing increased then decreased as the bolus washed out. The area under these signal attenuation curves are proportional to the relative blood volume. In 1990, Belliveau and colleagues took this one step further and mapped blood volume during rest and during activation (4). The first maps of brain activation using fMRI were demonstrated with this technique. As soon as the technique was demonstrated it was rendered obsolete (for brain activation imaging) by the use of an endogenous and oxygen-sensitive contrast agent: Hemoglobin.

27.2.2 Blood Oxygenation

As early as the 1930's it was known that hemoglobin was paramagnetic and deoxy-hemoglobin was diamagnetic (21). In 1982 it was discovered that changes in blood

oxygenation changed the T2 of blood, but it was not until 1989 that this knowledge was used to image in vivo changes in blood oxygenation (22). Blood oxygenation dependent contrast, coined BOLD by Ogawa et al. (23), was used to image the activated brain for the first time in 1991. Interestingly, Ogawa et al. predicted it's utility for functional brain imaging, but had predicted a signal *decrease* as opposed to a signal *increase*, as implied by some earlier PET results by Fox et al. (24) suggesting that the oxygen extraction fraction decreased during activation. The first results using BOLD contrast were published in 1992(13, 15, 23). Because of its sensitivity and ease of implementation, the contrast used to observe susceptibility changes with changes in blood oxygenation is the most commonly used functional brain imaging contrast used, and is the technique that will be primarily discussed in this chapter. The cascade of events that follow brain activation and lead to BOLD signal changes are shown in Figure 1.

27.2.3 Blood Perfusion

An array of new techniques exist for mapping cerebral blood *perfusion* in humans. Arterial spin labeling-based perfusion mapping MRI techniques are similar to those applied in other modalities such as positron emission tomography (PET) and single photon emission computed tomography (SPECT) in that they involve tagging inflowing blood, and then allowing flow of the tagged blood into the imaging plane. The RF tagging pulse is usually a 180° pulse that “inverts” the magnetization.

Generally, these techniques can be subdivided into those which use continuous arterial spin labeling, which involves continuously inverting blood flowing into the slice , and those which use pulsed arterial spin labeling, periodically inverting a block of arterial blood and measuring the arrival of that blood into the imaging slice. Examples these

techniques are “echo planar imaging with signal targeting and alternating RF” (EPISTAR) (25) and “flow-sensitive alternating inversion recovery,” (FAIR) (10, 26). Recently, a pulsed arterial spin labeling technique known as “quantitative imaging of perfusion using a single subtraction,” (QUIPSS), has been introduced (27).

27.2.4 Hemodynamic Specificity

With each of the above-mentioned techniques for imaging volume, oxygenation, and perfusion changes, the precise type of observable cerebrovascular information can be more finely delineated. While this information is typically more than the cognitive neuroscientist wants to know, it is useful to give an abbreviated summary of how specific MRI can actually be. Regarding susceptibility contrast imaging, spin-echo sequences are more sensitive to small susceptibility compartments (capillaries and red blood cells) and gradient-echo sequences are sensitive to susceptibility compartments of all sizes (28-31). Outer volume RF saturation removes inflowing spins (32), therefore reducing non-susceptibility related inflow changes when using short TR (with high flip angle) sequences. Diffusion weighting or “velocity nulling,” involving the use of $b > 50 \text{ s}^2/\text{mm}$, reduces the intravascular signal (33) therefore reducing, but not eliminating, large vessel effects (intravascular effects are removed but extravascular effects remain) in gradient-echo fMRI and all large vessel effects in spin-echo fMRI. Performing BOLD contrast fMRI at high field strengths has the same effect as diffusion weighting in the context of susceptibility - based contrast because the $T2^*$ and $T2$ of venous blood becomes increasingly shorter than the $T2^*$ and $T2$ of gray matter as field strength increases, therefore less signal will arise from venous blood at higher field strengths. (34). Figure 2 is a schematic diagram summarizing the pulse sequence selectivity of the specific aspects of the vasculature.

27.2.4 CMRO₂

Recently, advances in mapping activation-induced changes in the cerebral metabolic rate of oxygen (CMRO₂) using fMRI have developed (18, 20, 35-37). The basis for such measurement is that BOLD and perfusion contrast can be explained by the combination of a handful of parameters. The key then, is to either constrain the contrast or manipulate the physiologic state such that the number of parameters reduces to one or two. Normalization using a hypercapnia has evolved to be a method for mapping changes in CMRO₂ (18). The basic idea is that when the brain is activated, increases in flow, volume, and oxygenation are accompanied by an increase in CMRO₂. When a subject, at rest is undergoing a hypercapnic stress (5% CO₂), the cerebral flow, volume, and oxygenation increase without an accompanying increase in CMRO₂, therefore less oxygen is extracted from the blood stream, allowing the blood oxygenation change, relative to the perfusion change, to be greater than with brain activation. By comparing the ratio of the (simultaneously measured) perfusion and BOLD signal changes during hypercapnia and during brain activation, CMRO₂ information can be derived.

27.3 The Hemodynamic Transfer Function

The hemodynamic transfer function is referred to here as the combined effect on the fMRI signal change by the spatial and temporal variation in neuronal-vascular coupling, blood volume, blood flow, blood oxygenation, hematocrit, and vascular geometry, among other things. A goal of fMRI method development is to completely characterize this transfer function, (i.e. its spatial, temporal, pulse sequence, subject, physiologic, and pharmacological dependencies), so that more precise inferences can be made about underlying neuronal activation location, magnitude, and timing. The ultimate limits of fMRI depend on this characterization. This goal is particularly relevant in the context of understanding pharmacological effects on brain function.

After the onset of activation, or rather, after the neuronal firing rate has passed an integrated temporal-spatial threshold, either direct neuronal, metabolic, or neurotransmitter mediated signals reach arteriole sphincters, causing dilatation. The time for this initial process to occur is likely to be less than 100 ms. After vessel dilatation, the blood flow rate to increase by 10% to 200%. The time for blood to travel from arterial sphincters, through the capillary bed to pial veins is about 2 to 3 seconds. This transit time determines how rapidly the blood oxygenation saturation increases in each part of the vascular tree. As is shown in Figure 2, depending on the pulse sequence used, different aspects of the hemodynamics will manifest themselves.

27.3.1 Location

In resting state, hemoglobin oxygen saturation is about 95% in arteries and 60% in veins. The increase in hemoglobin saturation with activation is largest in veins, changing in saturation from about 60% to 90%. Likewise, capillary blood changes from about 80% to 90% saturation. Arterial blood, already saturated, shows no change. This large change in saturation is one reason why the strongest BOLD effect is usually seen in draining veins.

The second reason why the strongest BOLD effect is seen in draining veins is that activation - induced BOLD contrast is highly weighted by blood volume in each voxel. Since capillaries are much smaller than a typical imaging voxel, most voxels, regardless of size, will likely contain have about 2% to 4% capillary blood volume. In contrast, since the size and spacing of draining veins is on the same scale as most imaging voxels, it is likely that veins dominate the relative blood volume in any voxel that they pass through. Voxels that pial veins pass through can have 100% blood volume while voxels that contain no pial veins may have only 2% blood volume. This stratification in blood volume distribution strongly determines the magnitude of the BOLD signal.

As suggested in Figure 2, different pulse sequence weightings can give different locations of activation. For example, Figure 3 shows the activation in the motor cortex with two different functional MRI contrast weightings collected in the same plane – perfusion and BOLD. While much overlap is seen, the hot spots vary by as much as a 10 mm. The perfusion change map is sensitive primarily to *capillary* perfusion changes, while the BOLD contrast activation map is weighted mostly by veins. A potential worry regarding fMRI location is that venous blood, flowing away from the activated area, may maintain its elevated oxygen saturation as far as a centimeter away. When observing

brain activation on the scale of centimeters, this has not been a major concern. Nevertheless this issue will be discussed in detail later in the chapter.

27.3.2 Latency

One of the first observations made regarding fMRI signal changes is that, after activation, the BOLD signal takes about 2 to 3 seconds to begin to deviate from baseline(16, 38). Since BOLD signal is highly weighted towards venous oxygenation changes, with a flow increase, the time for venous oxygenation to begin to increase will be about the time that it takes blood to travel from arteries to capillaries and draining veins - 2 to 3 seconds. The hemodynamic “impulse response” function has been effectively used to characterize much of the BOLD signal change dynamics (39-41). This function has been derived empirically by performing very brief and well controlled stimuli. In addition it can be derived by deconvolving the neuronal input from the measured hemodynamic response(42, 43). This type of analysis assumes that the BOLD response behaves in a manner that can be completely described by linear systems analysis, which is still an open issue. Regardless, observed hemodynamic response to any neuronal activation can be predicted with a reasonable degree of accuracy, by convolving expected neuronal activity timing with the BOLD “impulse response” function. This function has typically been mathematically described by a Gamma Variate function (39).

If a task onset or duration is modulated, the accuracy to which one can correlate the modulated input parameters to the measured output signal depends on the variability of the signal within a voxel or region of interest. In a study by Savoy et al. (44)

addressing this issue, variability of several temporal sections of an activation -induced response were determined. Six subjects were studied, and for each subject, ten activation - induced response curves were analyzed. The relative onsets were determined by finding the latency with which the correlation coefficient was maximized with each of three reference functions, representing three parts of the response curve: the entire curve, the rising section, and the falling section. The standard deviation of the whole curve, rising phase, and falling phase were found to be 650 ms, 1250 ms, and 450 ms respectively.

Across - region differences in the onset and return to baseline of the BOLD signal during cognitive tasks have been observed. For example, during an visually - presented event - related word stem completion task Buckner et al. (45) reported that the signal in visual cortex increased about 1 sec before the signal in the left anterior prefrontal cortex. One might argue that this observation makes sense from a cognitive perspective since the subject first observes the word stem then, after about a second, generates a word to complete this task. Others would argue that the neuronal onset latencies should not be more than about 200 ms. Can inferences of the cascade of brain activation be made on this time scale from fMRI data? Without a method to constrain, or work around the intrinsic variability of the onset of BOLD signal over space, such inferences should not be made in temporal latency differences below about 4 sec.

Lee and Glover were the first to observe that the fMRI signal change onset within the visual cortex during simple visual stimulation varied from 6 sec to 12 sec (46). These latencies were also shown to correlate with the underlying vascular structure. The earliest onset of the signal change appeared to be in gray matter and the latest onset appeared to occur in the largest draining veins. Similar latency dispersions in motor cortex have been

observed. In one study, latency differences, detected in visual cortex using the Hilbert transform, did not show a clear correlation of latency with evidence for draining veins(47).

Figure 4 shows a summary of the sources of temporal variability. Figure 4a shows is a plot of the average time course from the motor cortex as a result of 2 sec finger tapping. As mentioned, the first source of variability is the intrinsic noise in the time series signal. The standard deviation of the signal is on the order of 1%. The second source of variability is that of the hemodynamic response. As mentioned, this ranges from 450 ms to 1250 ms depending on whether one is observing the rising phase of the signal or the falling phase. The third source of variability is the latency spread over space.

The plot in Figure 4a was used a reference function for correlation analysis and allowed to shift ± 2 sec. Figure 4b is a histogram of number of voxels in an activated region that demonstrated a maximum correlation with the reference function at each latency (relative to the average latency) to which the reference function was shifted. The spread in latencies is over 4 sec. Figure 4c includes a map of dot product (measure of signal change magnitude) and latency, that the regions showing the longest latency roughly correspond to the regions that show the largest signal changes. While these largest signal changes are likely downstream draining veins, it is important to note that this approximate correlation between latency and magnitude is extremely weak. Many very small signal changes show very long latencies. It is also interesting to note that the inverse, that many large signal changes show short latencies, is typically not true. This implies that many downstream vessels may be almost fully diluted back to resting state

oxygenation, therefore showing only a small signal change but still a large latency. Again, work is ongoing in better characterizing this effect.

27.3.3 Magnitude

As discussed above, the magnitude of the fMRI signal change is influenced by many variables which may vary across subjects, neuronal systems, within neuronal systems, and voxels. To make a complete and direct correlation between neuronal activity and fMRI signal change magnitude, in a single experiment, will remain impossible until all the variables can be characterized on a voxel-wise basis. Because of these primarily physiologic variables, brain activation maps will typically show a range of BOLD signal change magnitude from 1% to 5% (at say 1.5T, GE sequence, TE = 40 ms). The picture is not that bleak though. In the past several years, considerable progress has been made in characterizing the magnitude of the fMRI signal change with underlying neuronal activity.

The progressive series of studies are described as follows. First, as mentioned previously, it was clear that areas that showed significant BOLD signal change were in the appropriate neuronal area corresponding to specific well characterized tasks. Second, inferred neuronal modulation was carried out by systematically varying some aspect of the task. Clear correlations between BOLD signal change magnitude and visual flicker rate, contrast, word presentation rate, and finger tapping rate were observed(13, 48-50). This parametric experimental design represented a significant advance in the manner in which fMRI experiments were performed, enabling more precise inferences, not about

the BOLD signal change with task modulation. Still, of course, the degree of neuronal activation (i.e. integrated neuronal firing over a specified area) was still inferred.

Recently several more intriguing studies have emerged correlating measured neuronal firing rate with well known stimuli in animals (51) and humans(52, 53), demonstrating a remarkably high correlation between BOLD signal change and electrophysiologic measures.

27.3.4 Linearity

Close the topic of signal change magnitude is that of BOLD signal change linearity. It has been found that, with very brief stimulus durations, the BOLD response shows a larger signal change magnitude than expected if assuming that it behaves as a linear system (54, 55). This greater than expected BOLD signal change is generally specific to stimuli durations below 3 sec. Reasons for nonlinearities in the event-related response can be neuronal, hemodynamic, and/or metabolic in nature. The neuronal input may not be a simple boxcar function. Instead, an increased neuronal firing rate at the onset of stimulation (neuronal “bursting”) may cause a slightly larger amount of vasodilatation that later plateaus at a lower steady state level. The amount of neuronal bursting necessary to significantly change the hemodynamic response, assuming a linear neuronal-hemodynamic coupling, is quite large. For example, to account for the almost double functional contrast for the experimental relative to the linear convolution-derived single event responses, the integrated neuronal response over 2 s must double. Assuming

that neuronal firing is only at a higher rate for about the first 50 ms of brain activation, the neuronal firing rate must be 40 times greater than steady state for this duration.

BOLD contrast is highly sensitive to the interplay of blood flow, blood volume, and oxidative metabolic rate. If, with activation, any one of these variables changes with a different time constant, the fMRI signal may show fluctuations until a steady state is reached (56, 57). For instance, an activation - induced increase in blood volume would slightly reduce the fMRI signal since more deoxyhemoglobin would be present in the voxel. If the time constant for blood volume changes were slightly longer than that of flow changes, then the activation-induced fMRI signal would first increase then be reduced as blood volume later increased. The same could apply if the time constant of oxidative metabolic rate were slightly slower than that of flow and volume changes. Evidence for increased oxidative metabolic rate after 2 minutes of activation is given by Frahm (57), but no evidence suggests that the time constant of the increase in oxidative metabolic rate is only seconds longer than the flow increase time constant—as would be required to be applicable only to relatively high amplitude single event responses. These hemodynamics, which may also differ on a voxel wise basis, remain to be characterized fully.

27.4 Scanner Related Issues

A complete discussion of all scanner related issues and potential solutions is beyond the scope of this chapter. A rudimentary yet necessary description of the most basic problems and solutions is described in the following sections. Most functional MRI practitioners typically undergo a painful, frustrating, and prolonged period of learning about all of the scanner related limitations and issues. Some give up hope completely. The determined usually emerge hopeful again, and with a much better “feel” for what can and can’t be done from a brain imaging perspective. This learning process also takes place in understanding the physiology of the signal, but typically the most anguish arises in the context of MRI pulse sequences and hardware.

To start out, each of the categories listed below are more or less linked. In this section, an attempt is made to informally walk through the tradeoffs and issues involved with the nuts and bolts of performing an fMRI experiment.

27.4.1 Acquisition Rate

Image acquisition rate is ultimately limited by how fast the signal can be digitized and by how rapidly the imaging gradients can be switched. MR imaging can be logically divided into single-shot and multi-shot techniques. In single-shot imaging, spins are excited with a single excitation pulse and all the data necessary for creation of an image is collected at once. Echo planar imaging is the most common single shot technique. (With one “echo” a single “plane” is acquired). Multi-shot techniques are the most

commonly used for high resolution anatomical imaging. In clinical scanning (using multi-shot imaging), a single “line” of raw data is acquired with each RF excitation pulse. Because of the relatively long time it takes for the longitudinal magnetization to return to equilibrium (characterized by the T1 of the tissue), a certain amount of time, between 50 and 500 ms, is spent waiting between shots, otherwise, there would quickly be no signal left. It would be “saturated”. Because of this necessary waiting time, multi-shot techniques are typically slower than single shot techniques. For a 150 ms “waiting time” (or repetition time – TR), an image with 128 lines of raw data would take $150 \text{ ms} \times 128 = 19.2 \text{ sec}$.

In the case of echo-planar imaging, the entire data set for a plane is typically acquired in about 20 to 40 ms. In the context of performing a BOLD experiment, the echo time (TE) will be about 20 to 40 ms. Along with some additional time for applying other necessary gradients, the total time for an image to be acquired is about 60 to 100 ms, allowing 10 to 16 images to be acquired in a second. Improvements in digital sampling rates and gradient slew rates will allow small improvements, but essentially, this is about the upper limit for imaging humans.

In the context of an fMRI experiment with echo planar imaging, the typical image acquisition rate is determined by how many slices can temporally fit into a TR (repetition time). For whole brain imaging, approximately 20 slices (5 mm thickness) are required to cover the entire brain. This would allow a TR of about 1.25 to 2 sec. at minimum. This image collection rate is more than adequate to capture most of the details of the slow and dispersed hemodynamic response.

27.4.2 Spatial Resolution

The spatial resolution is also primarily determined by the gradient strength, the digitizing rate, and the time available. For multi shot imaging, as high resolution as desired can be achieved if one is willing to wait. One can keep on collecting lines of data with more RF pulses. For echo planar imaging, the signal decay rate (described by $T2^*$ with gradient-echo EPI and by $T2$ with spin-echo EPI) plays a significant role in determining the resolution. One can only sample for so long before the signal has completely decayed away. For this reason, echo planar images are generally much lower resolution than multi-shot images. To get around this problem, two further strategies are commonly used. The first is multi-shot EPI, in which the full EPI acquisition is used multiple times (but much fewer than with typical clinical multi-shot imaging), and interleaved in a fashion to increase the resolution. The second is to perform an operation called conjugate synthesis, which is basically making use of the fact that, in raw data space, half of the data is redundant. This allows at most, twice the resolution, with some cost in signal to noise and image quality. An example of multishot EPI is shown in Figure 5.

27.4.3 Signal to Noise

The signal to noise and the functional contrast to noise are influenced by many variables. These include, among other things, voxel volume, echo time (TE), repetition time (TR), flip angle, receiver bandwidth, field strength, and RF coil used. Not

considering fMRI for a moment, the image signal to noise is increased with larger voxel volume, shorter echo time, longer repetition time, larger flip angle (to 90°), narrow receiver bandwidth, higher field strength, and smaller RF coil. That said, in the context of fMRI, the functional contrast to noise is optimized with a voxel volume equaling the size of the activated area, $TE \approx \text{gray matter } T2^*$, short TR (optimizing samples per unit time), flip angle = Ernst angle = $\cos(-TR/T1)$, narrow receiver bandwidth, high field strength, and smaller RF coil. Of course, all of these variables come at some expense to others.

27.4.4 Stability

Theoretically, the noise, if purely thermal in nature, should propagate similarly over space and across time. In fMRI this is not at all the case since each image is essentially captured in 40 ms and the time series is collected in minutes. Stability is much more of an issue on the longer time scale. Flow and motion are correlated in many areas with cardiac and respiratory cycles. Subject movement and scanner instabilities also contribute. Single shot techniques have generally better temporal stability than multishot techniques since, with multishot techniques, the image is collected over a larger time scale, allowing for instabilities on a longer time scale enter into the image creation itself. This leads to non-repeatable ghosting patterns which general decreases temporal signal to noise ratio. Work is ongoing to characterize and reduce temporal instabilities for both single and multi – shot imaging(58) techniques(59). Correction techniques include cardiac gating(60), navigator pulses(61, 62), and raw data reordering(63, 64).

27.4.5 Image quality

Image quality issues that are the most prevalent are image warping and signal dropout. While books can be written on this subject, the description here is kept to the bare essentials.

Image warping is fundamentally caused by one or both of two things, B_0 field inhomogeneities and gradient nonlinearities. A non linear gradient will cause nonlinearities in spatial encoding, causing the image to be distorted. This is primarily a problem when using local, small gradient coils that have a small region of linearity that drops off rapidly at the base and top of the brain. With the growing prevalence of whole body gradient-coils for performing echo planar imaging, this problem is no longer a major issue. If the B_0 field is inhomogeneous, as is typically the situation with imperfect shimming procedures – particularly at higher field strengths, the protons will be processing at different frequencies than expected in their particular location. This will cause image deformation in these areas of poor shim – particularly with long readout window or acquisition time of echo planar imaging. A solution to this is to either shim better(65, 66) or map the B_0 field and perform a correction based on this map(67).

Signal dropout is related to the above problem in that it is also caused by localized B_0 field inhomogeneities, typically at interfaces of tissues having different susceptibilities. If within a voxel, because of the B_0 inhomogeneities, spins are spinning at different frequencies, their signals will cancel each other out. Several strategies exist for reducing this problem. One is, again, to shim as well as possible at the desired area. Due to still imperfect shimming procedures, this usually is not satisfactory. The other is

to reduce the voxel size (increase the resolution), thereby having less of a stratification of different frequencies within a voxel. The third is to choose the slice orientation such that the smallest voxel dimension (in many studies, the slice thickness is greater than the in-plane voxel dimension) is orientated perpendicular to the largest B_0 gradient. Because of this, many studies are performed using sagittal or coronal slice orientations.

As with many of the topics discussed, much more can be said, but the goal here is to simply give an introduction and a reference to more reading material.

27.5 Best Results So Far

The primary discussion, up to this point has been on the limits imposed by the scanner and the hemodynamics. This section is a discussion of some of the most successful, thought-provoking, and innovative fMRI studies, from a methodological perspective, as of Sept, 2000. The best results in temporal resolution and spatial resolution are presented.

27.5.1 Temporal Resolution

As discussed in previous sections of this chapter, MR images can be acquired at an extremely rapid rate, therefore, scanner-related limits are not the prime determinant of the upper limits on the temporal resolution of fMRI. The key to pushing the temporal resolution in fMRI is to either better characterize the hemodynamic response or to work around it's limits. The results described here are examples of this work over the past few years.

To obtain information about relative onsets of cascaded neuronal activity from hemodynamic latency maps,. It is possible to determine *relative* latency changes on modulation of the task timing. Savoy et al. (68) demonstrated that activation onset latencies of 500 ms were discernible using a visual stimulation paradigm in which the left and right hemifields were stimulated at relative delays of 500 ms. First, the subject viewed a fixation point for 10 sec. Then, the subject's left visual hemifield was activated

500 ms before the right. Both hemifields were activated for 10 sec, then the left hemifield stimulus was turned off 500 before the right.

While, with careful choice of ROI from which the time course plot is made, these onset differences can be shown, maps of latency cannot reveal the onset differences because, as mentioned, the variability over space, which is about 4 sec, dominates the inserted 500 ms variability from left to right hemifield.

To *map* the relative latency differences between hemifields, it is necessary to modulate the relative stimulation timing. As of an extension to their results, the left - right onset order was switched so that, in the second run, the right hemifield was activated and turned off 500 ms prior to the left. Latency maps were made for each onset order and subtracted from each other to reveal clear delineation between right and left hemifield that was not apparent in each of the individual maps. This operation and the resulting *relative* latency map is shown in Figure 6. These maps are of the change in onset of one area relative to another and not of absolute latency. It is also useful to note that the standard deviation of these maps is reduced to simply the standard deviation of the latencies in each voxel and not the standard deviation of the latencies over space. Maps such as these may be extremely useful in determining which regions of activation are modulated relative to other areas with a specific task timing modulation.

Published work by Menon et al. (69), Kim et al. (70), and Richter et al.(71) and Bandettini et al. (72) have explored the temporal resolution limits of fMRI. The results of Menon et al. (69), similar to those mentioned above, concluded that relative brain activation timings on the order of 50 ms can be discerned.

In Richter et al, an parametrically varied event- related mental rotation task was used. Each mental rotation task was presented individually. A high correlation between task duration and event-related width was demonstrated. The longer the task took to

accomplish, (larger rotation angle) the wider the event-related response was shown to be specific parietal locations.

27.5.2 Spatial Resolution

The hemodynamic point spread function was first considered and characterized by Engel et al. (73-75). Localization to 1.1 mm was determined.

The first successful mapping of ocular dominance columns in humans was published by Menon et al. to has published a series of papers describing this. He recently has shown intriguing results showing that the optimal way to pull out differences in activation across closely spaced units is by performing very brief stimuli so as to not reduce the dynamic range of the oxygenated blood that is flowing away beyond the unit of activation.

From an MRI pulse sequence perspective, it is important to note that to map cortical columns multi-shot imaging(76) is required. Performance of multi-shot imaging requires either navigator echoes or shot to shot phase correction schemes. If this is not performed, temporal stability is seriously compromised.

Many have argued that the some aspects of the BOLD signal change dynamics are more spatially localized to neuronal activity. Specifically, the evasive “pre-undershoot” has been indicated as such(77, 78). The rationale is that this transient “dip” in the signal that occurs 0.5 to 2 sec after the onset of activation and quickly gives way to the much larger signal increase is due to direct extraction of oxygen from the blood by adjacent activated tissue. Recently published work has demonstrated the utility of such an approach for mapping cortical columns in animals (79-81).

The highest resolution functional MRI performed with single shot EPI was carried out by Jesmanowicz et al. (82). Here a partial k-space strategy was used to obtain a presumed 256 x 256 resolution. The actual resolution achieved is debatable because of T2* effects reducing the resolution below that implied by the matrix size.

27.6 Neuronal Activation Input Strategies

So far, much of the chapter has been devoted to the basics and some esoteric issues regarding fMRI. This section is more of an overview of the types of neuronal input strategies that have been used to optimally use fMRI to extract information about what the brain is doing. Given a question of brain function, what are the available strategies that one can use to design their paradigm? A schematic summary of these strategies is shown in Figure 7.

27.6.1 Block Design

A block design paradigm was the first used in fMRI and is still the most prevalent neuronal input strategy. Borrowed from previous positron emission tomography studies, it involves having a subject perform a task for at least 10 seconds, alternated with a similar time for a control task, so that the hemodynamic response reaches a steady state in each condition. This is a useful technique in that it is easy to implement and standard statistical tests can be used to compare each condition.

27.6.2 Phase and Frequency Encoding

Phase encoding a stimuli involves varying some aspect of the stimuli in a continuous and cyclic manner. This strategy has been most successfully used in performing retinotopic mapping(75, 83, 84). In this type of study, a visual stimulus ring is

continuously varied in eccentricity, then, after the most extreme eccentricity is reached, the cycle is repeated again. The data are then typically analyzed using Fourier analysis, mapping out the areas that show a signal change temporal phase that correlates with the stimulus phase. This is a powerful technique since it makes use of the entire time series in that there are no “off” states. It is also lends itself to Fourier analysis - a powerful analysis technique. This method has also been used for somatotopic mapping(85), and tonotopic mapping(86).

Frequency encoding is much less common, but is achievable for certain types of stimuli. The method is to designate a specific on-off frequency for each type of stimulus used. Again, the use of Fourier analysis to analyze the data reveals the most power under a specific spectral peak corresponding to the brain area specific to the particular on-off frequency. The utility of this method has been demonstrated in the mapping of left and right motor cortex by cueing the subject to perform a finger tapping task at different on-off rates for each hand(87).

27.6.3 Orthogonal Designs

Orthogonal task design is a powerful extension of block design studies. The basic concept is that if one designs two different task timings that would create BOLD responses that are orthogonal to each other, then these tasks can be performed simultaneously during a single time series collection with no cross-task interference, making comparison much more precise. This technique was pioneered by Courtney et al.

(88). In their study, six orthogonal tasks were designed into a single time series. This type of design also lends itself to event-related studies.

27.6.4 Parametric Designs

As mentioned in section 27.3.3, parametric designs are powerful in that more precise statements can be made about relative neuronal activity. A parametric task design simply involves systematically varying some aspect of the task during the time series. This may be finger tapping rate, stimulus contrast or flicker rate, cognitive load, attention demand, etc. and, instead of mapping the magnitude of the change with a single task, mapping the slope of the change corresponding to a task. In this manner relative brain activation magnitude may be teased out of the time series.

27.6.5 Event-Related Designs

Before 1995, a critical question in event-related fMRI was whether a transient cognitive activation could elicit a significant and usable fMRI signal change. In 1996, Buckner et al. demonstrated that, in fact, event-related fMRI lent itself quite well to cognitive neuroscience questions(45). In their study, a word stem completion task was performed using a “block-design” strategy and an event-related strategy. Robust activation in the regions involved with word generation were observed in both cases.

Given the substantial amount of recently recent publications which use event-related fMRI(40-42, 65, 89-112), it can be probably said that this is one of the more exciting developments in fMRI since it's discovery.

The advantages of event-related activation strategies are many(113). These include the ability to more completely randomize task types in a time series(114-116), the ability to selectively analyze fMRI response data based on measured behavioral responses to individual trials(111), and the option to incorporate overt responses into a time series. Separation of motion artifact from BOLD changes is possible by the use of the temporal response differences between motion effects and the BOLD contrast-based changes(91).

When using a constant ISI, the optimal ISI is about 10 to 12 seconds. Dale and Buckner (43) have shown that responses to visual stimuli, presented as rapidly as once every 1 sec, can be adequately separated using overlap correction methods. Overlap correction methods are only possible if the ISI is varied during the time series. These results appear to demonstrate that the hemodynamic response is sufficiently linear to apply deconvolution methods to extract overlapping responses. Burock et al. (95) has demonstrated that remarkably clean activation maps can be created using an average ISI of 500 ms. Assuming the hemodynamic response is essentially a linear system, there appears to be no obvious minimum ISI when trying to estimate the hemodynamic response. Dale has suggested that an exponential distribution of ISI's, having a mean as short as psychophysically possible, is optimal for estimation(100). Of course the fastest one can present stimuli depends on the study being performed. Many cognitive tasks may require a slightly longer average presentation rate.

Future work in event-related experimental optimization rests in what further information can be derived from these responses. Between-region, between-voxel, between-subject, and stimulus-dependent variations in amplitude, latency, shape, and responsivity of the event-related fMRI responses are still relatively uncharacterized. Reasons for these differences are also still unclear.

27.6.6 Free Behavior Designs

For many types of cognitive neuroscience questions, it is not possible to precisely constrain the timing or performance of a task. It is necessary then to allow the subject to perform the task “freely” and take a continuous measurement of the performance, then use this measurement as a reference function for subsequent time series analysis. Examples of this type of design are emerging. As an example, the skin conductance changes are difficult to predict or control. In a study by Patterson et al. (117), skin conductance was simultaneously recorded during an array of tasks and during “rest.” The skin conductance signal change was then used as a reference function in the fMRI time series analysis. Several cortical and subcortical regions were shown to have signal changes that were highly correlated with the skin conductance changes. Without the use of this measurement, these signal changes would appear as noise. It is thought that this type of design will become more prevalent as methods to precisely monitor subject performance or state become more sophisticated.

27.7 Conclusion

This chapter is an attempt to combine a review of the fundamentals with a glimpse of fMRI state of the art. Starting with the basics of fMRI contrast, the discussion led into that of the hemodynamic transfer function – fundamental to understanding fMRI signal changes. Characteristics, all related to the hemodynamic transfer function; location, latency, magnitude, and linearity, were discussed. From here, the chapter deviated back into perhaps less provocative, but still important issues having to do with working with an MRI scanner and understanding some practical limitations. A sampling of best results, being those that successfully brought many of the previous topics into play in experimental design and analysis, were shown as examples. Lastly, the chapter ended with a brief overview of neuronal input strategies or, rather, ways in which one can activate the brain in the context of an fMRI experiment.

Functional MRI is about 9 years old and apparently still at the beginning of its growth curve, in terms of users and applications. Clinical applications are just beginning, while cognitive neuroscience applications are in full swing. The field of fMRI continues to develop along intertwining paths of understanding the signal, creating the tools, and refining the questions being asked.

Figure Captions

Figure 1. The cascade of hemodynamic and MRI events that occur following brain activation.

Figure 2. The vascular tree, including arteries (left), arterioles, capillaries, and veins (right). If the inside of the vessel drawing is filling in, the signal has an intravascular contribution. Arterial spin labeling (ASL) is differentially sensitive to the arterial-capillary region of the vasculature, depending on the TI used and whether or not velocity nulling (otherwise called diffusion weighting) gradients are used. A small amount of velocity nulling and a TI of about 1 sec makes ASL techniques selectively sensitive to capillaries. Susceptibility-based techniques, including gradient-echo (GE) and spin-echo (SE), are also differentially sensitive to specific aspects of the vasculature. GE techniques are sensitive to susceptibility perturbations of all sizes, therefore they are sensitive to all intravascular and extravascular effects. SE techniques are sensitive to susceptibility perturbations about the size of a red blood cell or capillary, making them sensitive to intravascular (IV) effects in vessels of all sizes and to extravascular capillary effects. Velocity nulling makes GE sequences sensitive to extravascular capillary to vein effects, and makes SE sequences selectively sensitive to only capillary effects.

Figure 3: Comparison of activation-induced signal changes in perfusion and BOLD measurements. Both measurements were obtained at 3T. Perfusion measurements were obtained using FAIR-EPI with TI = 1400 ms. BOLD measurements were obtained using GE-EPI with TE = 30 ms.

Figure 4: Demonstration of several of the limits of fMRI temporal resolution. Echo planar imaging was performed at 3 Tesla using a Bruker Biospec 3T/60 equipped with a local head gradient coil. An time course series of axial images (matrix size = 96 x 96, FOV = 20 cm, TE = 40 ms, TR = 500 ms, flip angle = 80°) through the motor cortex was obtained. Bilateral finger tapping was performed for 2 sec., alternating with 18 sec. rest. These figures demonstrate that the upper temporal resolution is determined by the variability of the signal change in time and space. **a.** Time course of the signal elicited by tapping fingers for 2 sec. The standard deviation at each point was in the range of 1 to 2%. The standard deviation of the hemodynamic change, in time, is in the range of 450 ms to 650 ms. **b.** Map of the dot product (a measure of the activation - induced signal change magnitude) and the relative latencies or delays of the reference function (the plot in a. was used as the reference function) at which the correlation coefficient was maximized. The spatial distribution of hemodynamic delays has a standard deviation of about 900 ms. The longest delays approximately match the regions that show the highest dot product and the area where veins are shown as dark lines in the T2*

weighted anatomical image. **c.** Histogram of relative hemodynamic latencies. This was created from the latency map in b.

Figure 5: An example of multi shot EPI. Number of excitations ranged from 1 to 8. The image resolution increases but the signal to noise and functional contrast to noise decreases. In addition, instabilities are introduced into the time course by the use of multi shot imaging.

Figure 6: The use of latency maps and task modulation to extract relative latencies. Activation within a region of visual cortex is shown. In one condition, (left), the right visual hemifield stimulation precedes the left by 500 ms. In the other condition, (middle), the left visual hemifield precedes the right hemifield stimulation by 500 ms. Latency maps from both these conditions show an across-voxel spread of ± 2.5 sec which is too large to clearly identify the relative latencies across hemifields. However, once the data are normalized for this intrinsic variance by directly comparing the hemodynamic response from the two different lags within individual voxels, the offset between left and right hemifield can be observed (right). This is a demonstration that suggests that normalization of the hemodynamic lag can allow small relative temporal offsets to be identified. These normalized offsets can then be compared across regions to make inferences about neuronal delay. For this experiment, the TR was 400 ms.

Figure 7: Overview and schematic depiction of types of neuronal input strategies available in fMRI. In addition, parametric designs, which involve systematically varying some aspect of the intensity of the neuronal input, can be applied to any of the design strategies.

References

1. **Rosen BR, Belliveau JW, Aronen HJ, et al.** Susceptibility contrast imaging of cerebral blood volume: human experience. *Magn. Reson. Med.* 1991;22:293-299.
2. **Rosen BR, Belliveau JW, Chien D.** Perfusion imaging by nuclear magnetic resonance. *Magn. Reson. Quart.* 1989;5:263-281.
3. **Moonen CTW, vanZijl PCM, Frank JA, LeBihan D, Becker ED.** Functional Magnetic Resonance Imaging in Medicine and Physiology. *Science.* 1990;250:53-61.
4. **Belliveau JW, Kennedy DN, McKinstry RC, et al.** Functional mapping of the human visual cortex by magnetic resonance imaging. *Science.* 1991;254:716-719.
5. **Williams DS, Detre JA, Leigh JS, Koretsky AS.** Magnetic resonance imaging of perfusion using spin-inversion of arterial water. *Proc. Natl. Acad. Sci. USA.* 1992;89:212-216.
6. **Detre JA, Leigh JS, Williams DS, Koretsky AP.** Perfusion imaging. *Magn. Reson. Med.* 1992;23:37-45.
7. **Edelman RR, Sievert B, Wielopolski P, Pearlman J, Warach S.** Noninvasive mapping of cerebral perfusion by using EPISTAR MR angiography. *JMRI.* 1994; 4(P), [Abstr.]:68.
8. **Kwong KK, Chesler DA, Weisskoff RM, Rosen BR.** Perfusion MR imaging. *Proc., SMR, 2nd Annual Meeting. San Francisco; 1994: 1005.*

9. **Wong EC, Buxton RB, Frank LR.** Implementation of quantitative perfusion imaging techniques for functional brain mapping using pulsed arterial spin labeling. *NMR in Biomedicine*. 1997;10:237-249.
10. **Kim S-G.** Quantification of relative cerebral blood flow change by flow-sensitive alternating inversion recovery (FAIR) technique: application to functional mapping. *Magn. Reson. Med*. 1995;34:293-301.
11. **Ogawa S, Lee TM, Kay AR, Tank DW.** Brain magnetic resonance imaging with contrast dependent on blood oxygenation. *Proc. Natl. Acad. Sci. USA*. 1990;87:9868-9872.
12. **Turner R, LeBihan D, Moonen CTW, Despres D, Frank J.** Echo-planar time course MRI of cat brain oxygenation changes. *Magn. Reson. Med*. 1991;22:159-166.
13. **Kwong KK, Belliveau JW, Chesler DA, et al.** Dynamic magnetic resonance imaging of human brain activity during primary sensory stimulation. *Proc. Natl. Acad. Sci. USA*. 1992;89: 5675-5679.
14. **Ogawa S, Lee TM.** Functional brain imaging with physiologically sensitive image signals. *JMRI*. 1992;2(P)-WIP suppliment, [Abstr.]:S22.
15. **Bandettini PA, Wong EC, Hinks RS, Tikofsky RS, Hyde JS.** Time course EPI of human brain function during task activation. *Magn. Reson. Med*. 1992;25:390-397.
16. **Frahm J, Bruhn H, Merboldt K-D, Hanicke W, Math D.** Dynamic MR imaging of human brain oxygenation during rest and photic stimulation. *J. Magn. Reson. Imaging*. 1992;2:501-505.

17. **Haacke EM, Lai S, Reichenbach JR, et al.** In vivo measurement of blood oxygen saturation using magnetic resonance imaging: a direct validation of the blood oxygen level-dependent concept in functional brain imaging. *Human Brain Mapping*. 1997;5:341-346.
18. **Davis TL, Kwong KK, Weisskoff RM, Rosen BR.** Calibrated functional MRI: Mapping the dynamics of oxidative metabolism. *Proc. Natl. Acad. Sci. USA*. 1998;95:1834-1839.
19. **Kim S-G, Ugurbil K.** Comparison of blood oxygenation and cerebral blood flow effects in fMRI: estimation of relative oxygen consumption change. *Magn. Reson. Med*. 1997;38:59-65.
20. **vanZijl PCM, Eleff SM, Ulatowski JA, et al.** Quantitative assessment of blood flow, blood volume, and blood oxygenation effects in functional magnetic resonance imaging. *Nature Medicine*. 1998;4(2):159-166.
21. **Pauling L, Coryell CD.** The magnetic properties and structure of hemoglobin, oxyhemoglobin, and carbonmonoxyhemoglobin. *Proc. Natl. Acad. Sci. USA*. 1936;22:210-216.
22. **Thulborn KR, Waterton JC, Matthews PM, Radda GK.** Oxygenation dependence of the transverse relaxation time of water protons in whole blood at high field. *Biochim. Biophys. Acta*. 1982;714:265-270.
23. **Ogawa S, Tank DW, Menon R, et al.** Intrinsic signal changes accompanying sensory stimulation: functional brain mapping with magnetic resonance imaging. *Proc. Natl. Acad. Sci. USA*. 1992; 89:5951-5955.

24. **Fox PT, Raichle ME.** Focal physiological uncoupling of cerebral blood flow and oxidative metabolism during somatosensory stimulation in human subjects. *Proc. Natl. Acad. Sci. USA.* 1986;83:1140-1144.
25. **Edelman R, Siewert B, Darby D.** Qualitative mapping of cerebral blood flow and functional localization with echo planar MR imaging and signal targeting with alternating radiofrequency (EPISTAR). *Radiology.* 1994;192:1-8.
26. **Kwong KK, Chesler DA, Weisskoff RM, et al.** MR perfusion studies with T1-weighted echo planar imaging. *Magn Reson Med.* 1995;34(6):878-87.
27. **Wong EC, Buxton RB, Frank LR.** Quantitative imaging of perfusion using a single subtraction (QUIPSS and QUIPSS II). *Magnetic Resonance in Medicine.* 1998;39(5):702-8.
28. **Ogawa S, Menon RS, Tank DW, et al.** Functional brain mapping by blood oxygenation level - dependent contrast magnetic resonance imaging: a comparison of signal characteristics with a biophysical model. *Biophysical J.* 1993;64:803-812.
29. **Boxerman JL, Hamberg LM, Rosen BR, Weisskoff RM.** MR contrast due to intravascular magnetic susceptibility perturbations. *Magn. Reson. Med.* 1995;34:555-566.
30. **Kennan RP, Zhong J, Gore JC.** Intravascular susceptibility contrast mechanisms in tissues. *Magn. Reson. Med.* 1994;31:9-21.
31. **Bandettini PA, Wong EC.** Effects of Biophysical and physiologic parameters on brain activation-induced R2* and R2 changes: simulations using a deterministic

- diffusion model. *International Journal of Imaging Systems and Technology*. 1995;6:134-152.
32. **Duyn JH, Moonen CTW, vanYperen GH, Boer RWd, Luyten PR.** Inflow versus deoxyhemoglobin effects in BOLD functional MRI using gradient-echoes at 1.5 T. *NMR in Biomedicine*. 1994;7:83-88.
 33. **Boxerman JL, Bandettini PA, Kwong KK, et al.** The intravascular contribution to fMRI signal change: Monte Carlo modeling and diffusion-weighted studies in vivo. *Magn. Reson. Med*. 1995;34:4-10.
 34. **Menon RS, Ogawa S, Tank DW, Ugurbil K.** 4 tesla gradient recalled echo characteristics of photic stimulation - induced signal changes in the human primary visual cortex. *Magn. Reson. Med*. 1993;30:380-386.
 35. **Kim SG, Rostrup E, Larsson HB, Ogawa S, Paulson OB.** Determination of relative CMRO₂ from CBF and BOLD changes: significant increase of oxygen consumption rate during visual stimulation. *Magn Reson Med*. 1999;41(6):1152-61.
 36. **Hoge RD, Atkinson J, Gill B, Crelier GR, Marrett S, Pike GB.** Investigation of BOLD signal dependence on cerebral blood flow and oxygen consumption: the deoxyhemoglobin dilution model. *Magn Reson Med*. 1999;42(5):849-63.
 37. **Hoge RD, Atkinson J, Gill B, Crelier GR, Marrett S, Pike GB.** Stimulus-dependent BOLD and perfusion dynamics in human V1. *Neuroimage*. 1999;9(6 Pt 1):573-85.

38. **Bandettini PA.** MRI studies of brain activation: dynamic characteristics. *Functional MRI of the Brain*. Berkeley: Society of Magnetic Resonance in Medicine; 1993:143.
39. **Cohen MS.** Parametric analysis of fMRI data using linear systems methods. *NeuroImage*. 1997;6:93-103.
40. **Josephs O, Turner R, Friston K.** Event-related fMRI. *Human Brain Mapping*. 1997;5:243-248.
41. **Friston KJ, Josephs O, Rees G, Turner R.** Nonlinear event-related responses in fMRI. *Magn. Reson. Med.* 1998;39:41-52.
42. **Glover GH.** Deconvolution of impulse response in event-related BOLD fMRI. *Neuroimage*. 1999;9(4):416-29.
43. **Dale AM, Buckner RL.** Selective averaging of rapidly presented individual trials using fMRI. *Human Brain Mapping*. 1997;5:329-340.
44. **Savoy RL, O'Craven KM, Weisskoff RM, Davis TL, Baker J, Rosen B.** Exploring the temporal boundaries of fMRI: measuring responses to very brief visual stimuli. Book of Abstracts, Soc. for Neuroscience 24th Annual Meeting. Miami; 1994: 1264.
45. **Buckner RL, Bandettini PA, O'Craven KM, et al.** Detection of cortical activation during averaged single trials of a cognitive task using functional magnetic resonance imaging. *Proc. Natl. Acad. Sci. USA*. 1996;93(25):14878-83.
46. **Lee AT, Glover GH, Meyer CH.** Discrimination of large venous vessels in time-course spiral blood-oxygen-level-dependent magnetic-resonance functional neuroimaging. *Magn. Reson. Med.* 1995;33:745 -754.

47. **Saad ZS, DeYoe EA.** Time delay estimates of fMRI signals: efficient algorithm & estimate variance. Proc. 19th annual international conference IEEE/EMBS. Chicago; 1997: 460-463.
48. **Tootell RB, Reppas JB, Kwong KK, et al.** Functional analysis of human MT and related visual cortical areas using magnetic resonance imaging. *Journal of Neuroscience*. 1995;15(4):3215-30.
49. **Binder JR, Rao SM, Hammeke TA, Frost JA, Bandettini PA, Hyde JS.** Effects of stimulus rate on signal response during functional magnetic resonance imaging of auditory cortex. *Cognitive Brain Research*. 1994;2:31-38.
50. **Rao SM, Bandettini PA, Binder JR, et al.** Relationship between finger movement rate and functional magnetic resonance signal change in human primary motor cortex. *J. Cereb. Blood Flow and Metab*. 1996;16:1250-1254.
51. **Disbrow EA, Slutsky DA, Roberts TP, Krubitzer LA.** Functional MRI at 1.5 tesla: A comparison of the blood oxygenation level-dependent signal and electrophysiology [In Process Citation]. *Proc Natl Acad Sci U S A*. 2000;97(17):9718-23.
52. **Rees G, Friston K, Koch C.** A direct quantitative relationship between the functional properties of human and macaque V5. *Nat Neurosci*. 2000;3(7):716-723.
53. **Heeger DJ, Huk AC, Geisler WS, Albrecht DG.** Spikes versus BOLD: what does neuroimaging tell us about neuronal activity? [news; comment]. *Nat Neurosci*. 2000;3(7):631-3.

54. **Boynton GM, Engel SA, Glover GH, Heeger DJ.** Linear systems analysis of functional magnetic resonance imaging in human V1. *J. Neurosci.* 1996;16:4207-4221.
55. **Vazquez AL, Noll DC.** Nonlinear aspects of the BOLD response in functional MRI. *Neuroimage.* 1998;7(2):108-18.
56. **Buxton RB, Wong EC, Frank LR.** A biomechanical interpretation of the BOLD signal time course: the balloon model. Proc., ISMRM 5th Annual Meeting. Vancouver; 1997.
57. **Frahm J, Krüger G, Merboldt K-D, Kleinschmidt A.** Dynamic uncoupling and recoupling of perfusion and oxidative metabolism during focal activation in man. *Magn. Reson. Med.* 1996;35:143-148.
58. **Noll DC, Genovese CR, Vazquez AL, O'Brien JL, Eddy WF.** Evaluation of respiratory artifact correction techniques in multishot spiral functional MRI using receiver operator characteristic analyses. *Magn Reson Med.* 1998;40(4):633-9.
59. **Jezzard P.** Physiological Noise: Strategies for Correction. In: Moonen CTW, Bandettini PA, eds. *Functional MRI*. Berlin: Springer; 1999:173-181.
60. **Guimaraes AR, Melcher JR, Talavage TM, et al.** Imaging subcortical auditory activity in humans. *Hum Brain Mapp.* 1998;6(1):33-41.
61. **Lee CC, Jack CR, Jr., Grimm RC, et al.** Real-time adaptive motion correction in functional MRI. *Magn Reson Med.* 1996;36(3):436-44.
62. **Hu X, Kim S-G.** Reduction of signal fluctuations in functional MRI using navigator echoes. *Magn. Reson. Med.* 1994;31:495-503.

63. **Le TH, Hu X.** Retrospective estimation and correction of physiological artifacts in fMRI by direct extraction of physiological activity from MR data. *Magn Reson Med.* 1996;35(3):290-8.
64. **Wowk B, McIntyre MC, Saunders JK.** k-Space detection and correction of physiological artifacts in fMRI. *Magn Reson Med.* 1997;38(6):1029-34.
65. **Constable RT, Carpentier A, Pugh K, Westerveld M, Oszunar Y, Spencer DD.** Investigation of the Human Hippocampal Formation Using a Randomized Event-Related Paradigm and Z-Shimmed Functional MRI. *Neuroimage.* 2000;12(1):55-62.
66. **Glover GH.** 3D z-shim method for reduction of susceptibility effects in BOLD fMRI. *Magn Reson Med.* 1999;42(2):290-9.
67. **Jezzard P, Balaban RS.** Correction for geometric distortion in echo planar images from B₀ field distortions. *Magn. Reson. Med.* 1995;34:65-73.
68. **Savoy RL, Bandettini PA, Weisskoff RM, et al.** Pushing the temporal resolution of fMRI: studies of very brief visual stimuli, onset variability and asynchrony, and stimulus-correlated changes in noise. Proc., SMR 3rd Annual Meeting. Nice; 1995: 450.
69. **Menon RS, Luknowsky DC, Gati JS.** Mental chronometry using latency-resolved functional MRI. *Proceedings of the National Academy of Sciences of the United States of America.* 1998;95(18):10902-7.
70. **Kim SG, Richter W, Ugurbil K.** Limitations of temporal resolution in functional MRI. *Magnetic Resonance in Medicine.* 1997;37(4):631-6.

71. **Richter W, Somorjai R, Summers R, et al.** Motor area activity during mental rotation studied by time-resolved single-trial fMRI. *J Cogn Neurosci*. 2000;12(2):310-20.
72. **Bandettini PA.** The temporal resolution of functional MRI. In: Moonen CTW, Bandettini PA, eds. *Functional MRI*. Berlin: Springer; 1999:205-220.
73. **Engel SA, Rumelhart DE, Wandell BA, et al.** fMRI of human visual cortex. *Nature*. 1994;369, 370 [erratum]:525, 106 [erratum].
74. **Engel SA, Rumelhart DE, Wandell BA, et al.** fMRI of human visual cortex [letter] [published erratum appears in *Nature* 1994 Jul 14;370(6485):106]. *Nature*. 1994;369(6481):525.
75. **Engel SA, Glover GH, Wandell BA.** Retinotopic organization in human visual cortex and the spatial precision of functional MRI. *Cerebral Cortex*. 1997;7(2):181-92.
76. **Menon RS, Thomas CG, Gati JS.** Investigation of BOLD contrast in fMRI using multi-shot EPI. *NMR in Biomedicine*. 1997;10(4-5):179-82.
77. **Hu X, Le TH, Ugurbil K.** Evaluation of the early response in fMRI in individual subjects using short stimulus duration. *Magn Reson Med*. 1997;37(6):877-84.
78. **Yacoub E, Hu X.** Detection of the early negative response in fMRI at 1.5 Tesla. *Magn Reson Med*. 1999;41(6):1088-92.
79. **Duong TQ, Kim DS, Ugurbil K, Kim SG.** Spatiotemporal dynamics of the BOLD fMRI signals: toward mapping submillimeter cortical columns using the early negative response [In Process Citation]. *Magn Reson Med*. 2000;44(2):231-42.

80. **Grinvald A, Slovín H, Vanzetta I.** Non-invasive visualization of cortical columns by fMRI [news; comment]. *Nat Neurosci.* 2000;3(2):105-7.
81. **Kim DS, Duong TQ, Kim SG.** High-resolution mapping of iso-orientation columns by fMRI [see comments]. *Nat Neurosci.* 2000;3(2):164-9.
82. **Jesmanowicz A, Bandettini PA, Hyde JS.** Single - shot half NEX 256 x 256 resolution EPI at 3 Tesla. Proc., ISMRM 5th Annual Meeting. Vancouver; 1997.
83. **Sereno MI, Dale AM, Reppas JR, et al.** Functional MRI reveals borders of multiple visual areas in humans. *Science.* 1995;268:889 - 893.
84. **DeYoe EA, Carman G, Bandettini P, et al.** Mapping striate and extrastriate areas in human cerebral cortex. *Proc. Natl. Acad. Sci.* 1996;93:2382 - 2386.
85. **Servos P, Zacks J, Rumelhart DE, Glover GH.** Somatotopy of the human arm using fMRI. *Neuroreport.* 1998;9(4):605-9.
86. **Talavage TM, Ledden PJ, Sereno MI, Benson RR, Rosen BR.** Preliminary fMRI evidence for tonotopicity in human auditory cortex. *Neuroimage.* 1996;3:S355.
87. **Bandettini PA, Jesmanowicz A, Wong EC, Hyde JS.** Processing strategies for time-course data sets in functional MRI of the human brain. *Magn. Reson. Med.* 1993;30:161-173.
88. **Courtney SM, Ungerleider LG, Keil K, Haxby JV.** Transient and sustained activity in a distributed neural system for human working memory. *Nature.* 1997;386:608-611.

89. **Bandettini PA, Cox RW.** Event-related fMRI contrast when using constant interstimulus interval: theory and experiment. *Magn Reson Med.* 2000;43(4):540-8.
90. **Belin P, Zatorre RJ, Hoge R, Evans AC, Pike B.** Event-related fMRI of the auditory cortex. *Neuroimage.* 1999;10(4):417-29.
91. **Birn RM, Bandettini PA, Cox RW, Shaker R.** Event-related fMRI of tasks involving brief motion. *Hum Brain Mapp.* 1999;7(2):106-14.
92. **Buckner RL.** Event-related fMRI and the hemodynamic response. *Hum Brain Mapp.* 1998;6(5-6):373-7.
93. **Buckner RL, Koutstaal W, Schacter DL, Dale AM, Rotte M, Rosen BR.** Functional-anatomic study of episodic retrieval. II. Selective averaging of event-related fMRI trials to test the retrieval success hypothesis. *Neuroimage.* 1998;7(3):163-75.
94. **Buckner RL, Goodman J, Burock M, et al.** Functional-anatomic correlates of object priming in humans revealed by rapid presentation event-related fMRI. *Neuron.* 1998;20(2):285-96.
95. **Burock MA, Buckner RL, Woldorff MG, Rosen BR, Dale AM.** Randomized event-related experimental designs allow for extremely rapid presentation rates using functional MRI. *Neuroreport.* 1998;9(16):3735-9.
96. **Clare S, Humberstone M, Hykin J, Blumhardt LD, Bowtell R, Morris P.** Detecting activations in event-related fMRI using analysis of variance. *Magn Reson Med.* 1999;42(6):1117-22.

97. **D'Esposito M, Postle BR, Ballard D, Lease J.** Maintenance versus manipulation of information held in working memory: an event-related fMRI study. *Brain Cogn.* 1999;41(1):66-86.
98. **D'Esposito M, Postle BR, Jonides J, Smith EE.** The neural substrate and temporal dynamics of interference effects in working memory as revealed by event-related functional MRI. *Proc Natl Acad Sci U S A.* 1999;96(13):7514-9.
99. **D'Esposito M, Zarahn E, Aguirre GK.** Event-related functional MRI: implications for cognitive psychology. *Psychol Bull.* 1999;125(1):155-64.
100. **Dale AM.** Optimal experimental design for event-related fMRI. *Hum Brain Mapp.* 1999;8(2-3):109-14.
101. **Davis KD, Kwan CL, Crawley AP, Mikulis DJ.** Event-related fMRI of pain: entering a new era in imaging pain. *Neuroreport.* 1998;9(13):3019-23.
102. **Friston KJ, Fletcher P, Josephs O, Holmes A, Rugg MD, Turner R.** Event-related fMRI: characterizing differential responses. *NeuroImage.* 1998;7:30-40.
103. **Friston KJ, Zarahn E, Josephs O, Henson RN, Dale AM.** Stochastic designs in event-related fMRI. *Neuroimage.* 1999;10(5):607-19.
104. **Josephs O, Henson RN.** Event-related functional magnetic resonance imaging: modelling, inference and optimization. *Philos Trans R Soc Lond B Biol Sci.* 1999;354(1387):1215-28.
105. **Kang AM, Constable RT, Gore JC, Avrutin S.** An event-related fMRI study of implicit phrase-level syntactic and semantic processing. *Neuroimage.* 1999;10(5):555-61.

106. **Kiehl KA, Liddle PF, Hopfinger JB.** Error processing and the rostral anterior cingulate: an event-related fMRI study. *Psychophysiology*. 2000;37(2):216-23.
107. **McCarthy G.** Event-related potentials and functional MRI: a comparison of localization in sensory, perceptual and cognitive tasks. *Electroencephalogr Clin Neurophysiol Suppl*. 1999;49:3-12.
108. **Pinel P, Le Clec HG, van de Moortele PF, Naccache L, Le Bihan D, Dehaene S.** Event-related fMRI analysis of the cerebral circuit for number comparison. *Neuroreport*. 1999;10(7):1473-9.
109. **Postle BR, D'Esposito M.** "What"-Then-Where" in visual working memory: an event-related fMRI study. *J Cogn Neurosci*. 1999;11(6):585-97.
110. **Rosen BR, Buckner RL, Dale AM.** Event-related functional MRI: past, present, and future. *Proc Natl Acad Sci U S A*. 1998;95(3):773-80.
111. **Schacter DL, Buckner RL, Koutstaal W, Dale AM, Rosen BR.** Late onset of anterior prefrontal activity during true and false recognition: an event-related fMRI study. *Neuroimage*. 1997;6(4):259-69.
112. **Schad LR, Wiener E, Baudendistel KT, Muller E, Lorenz WJ.** Event-related functional MR imaging of visual cortex stimulation at high temporal resolution using a standard 1.5 T imager. *Magn Reson Imaging*. 1995;13(6):899-901.
113. **Zarahn E, Aguirre G, D'Esposito M.** A trial-based experimental design for fMRI. *NeuroImage*. 1997;6:122-138.
114. **Clark VP, Maisog JM, Haxby JV.** fMRI study of face perception and memory using random stimulus sequences. *J Neurophysiol*. 1998;79(6):3257-65.

115. **Dale A, Buckner R.** Selective averaging of individual trials using fMRI. Third Intl. Conf. on Func. Mapping of the Human Brain. Copenhagen; 1997: S47.
116. **McCarthy G, Luby M, Gore J, Goldman-Rakic P.** Infrequent events transiently activate human prefrontal and parietal cortex as measured by functional MRI. *J. Neurophysiol.* 1997;77:1630-1634.
117. **Patterson J, Bandettini P, Ungerleider LG.** Simultaneous skin conductance measurement and fMRI during cognitive tasks: correlations of skin conductance activity with ventromedial prefrontal cortex (PFC) and orbitofrontal cortex (OFC) activity. Human Brain Mapping. San Antonio; 2000: 235.

BOLD Contrast in the Detection of Neuronal Activity

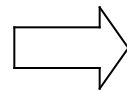
Cerebral Tissue Activation



Local Vasodilation



Increase in Cerebral Blood Flow and Volume



Oxygen Delivery Exceeds Metabolic Need



Increase in Capillary and Venous Blood Oxygenation

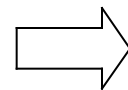


Decrease in Deoxy-hemoglobin

Deoxy-hemoglobin: paramagnetic
Oxy-hemoglobin: diamagnetic



Decrease in susceptibility-related intravoxel dephasing

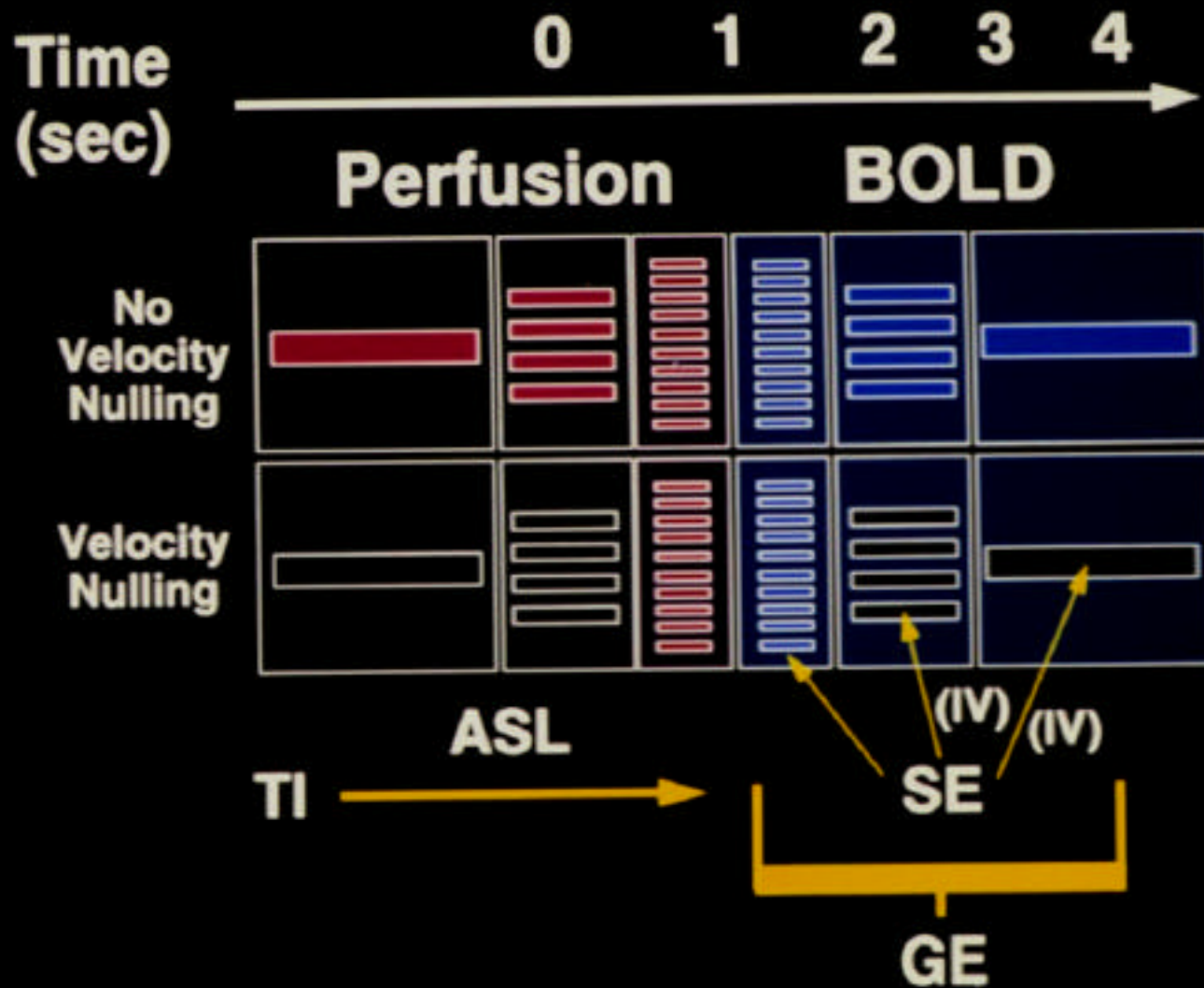


Increase in T2 and T2*

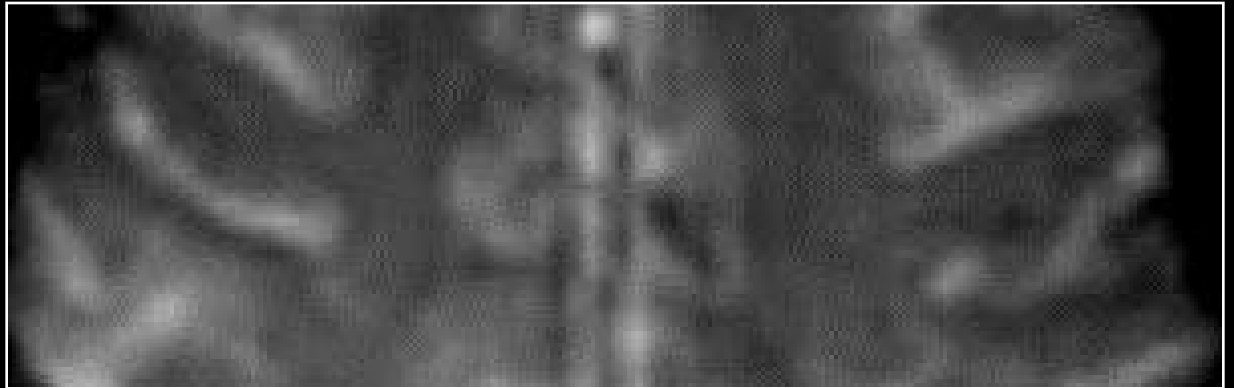


Local Signal Increase in T2 and T2* – weighted sequences

Hemodynamic Specificity



Anatomy

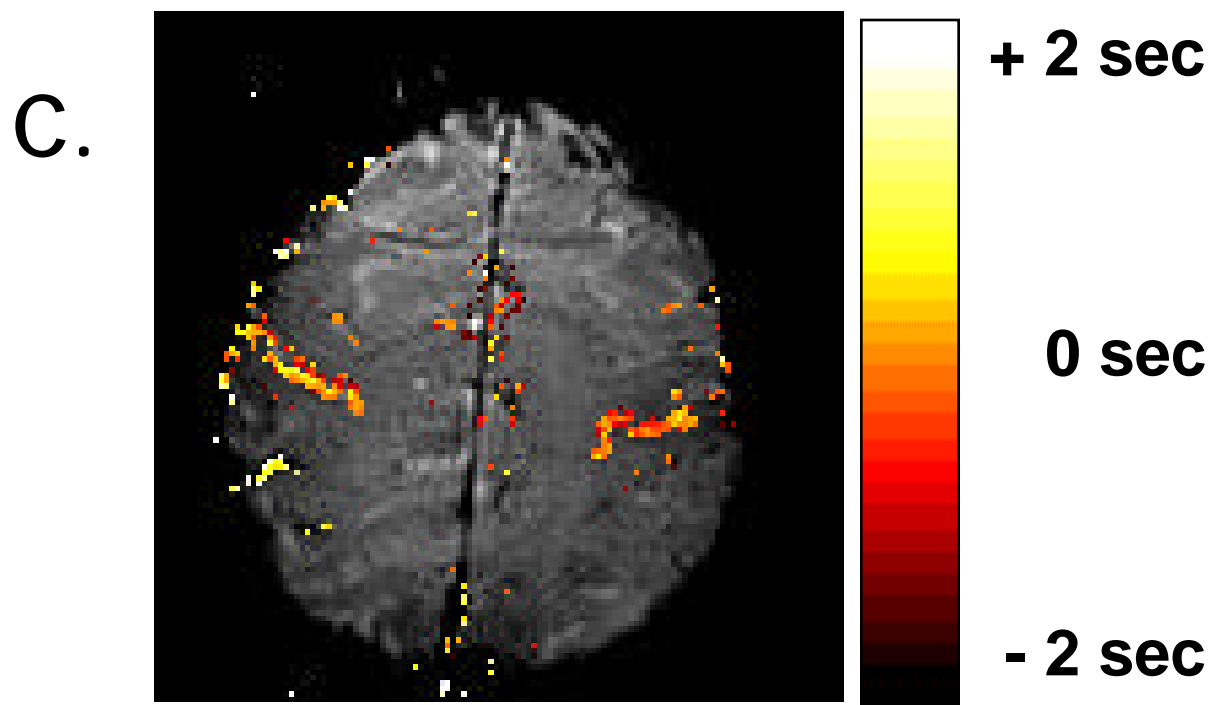
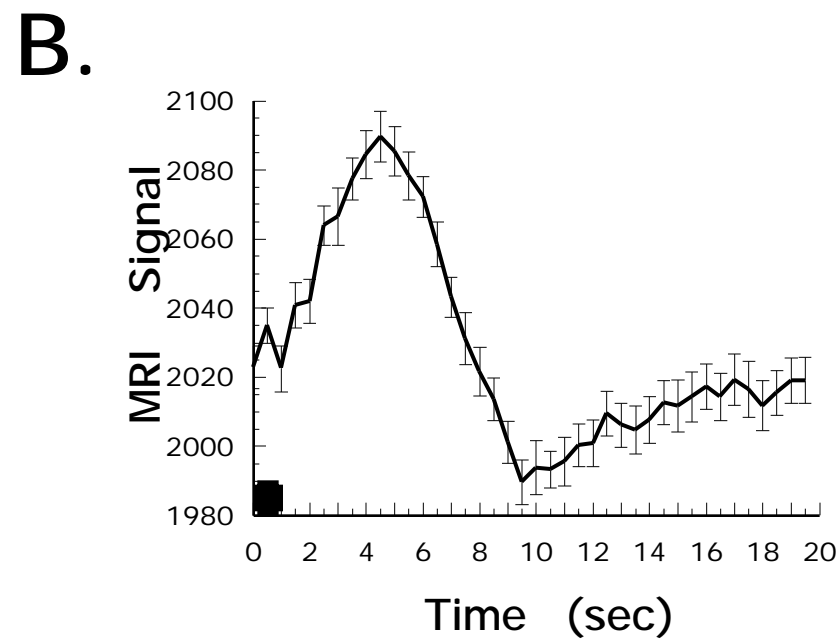
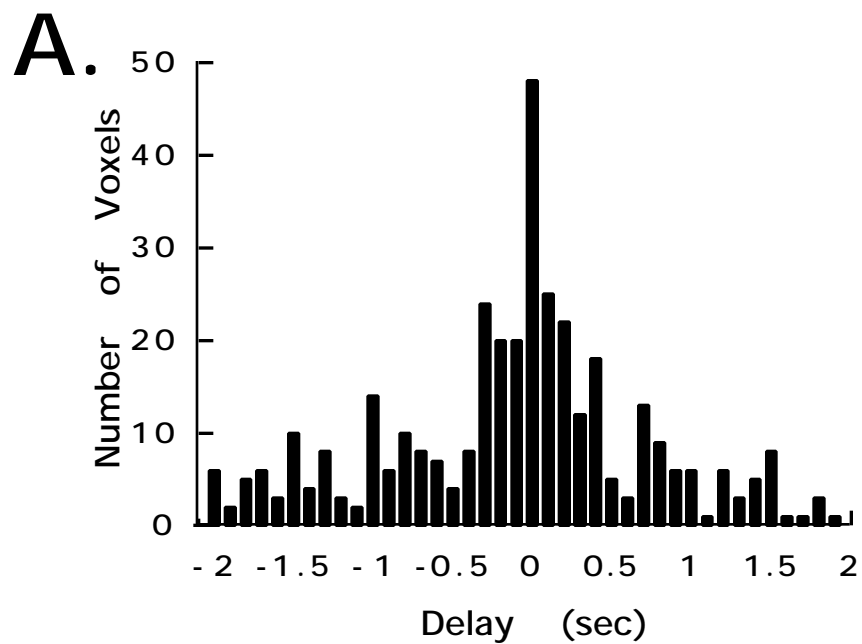


BOLD

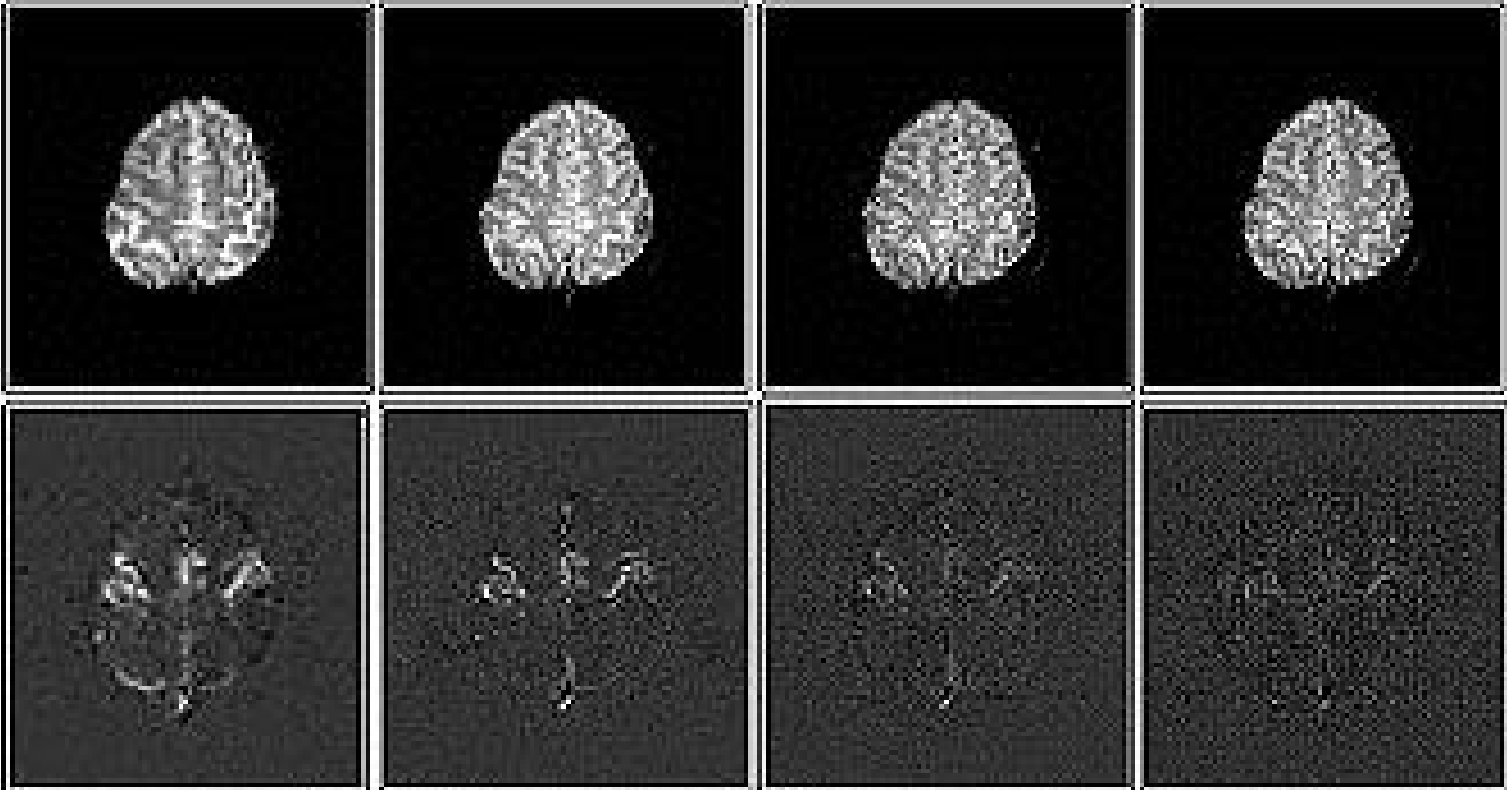


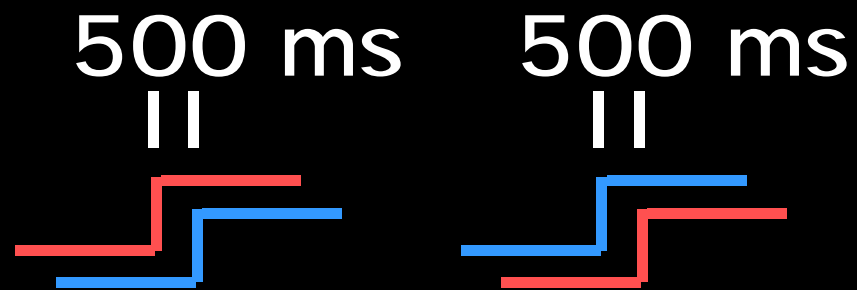
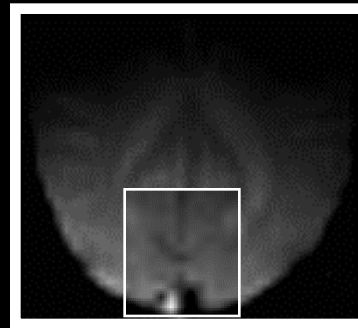
Perfusion



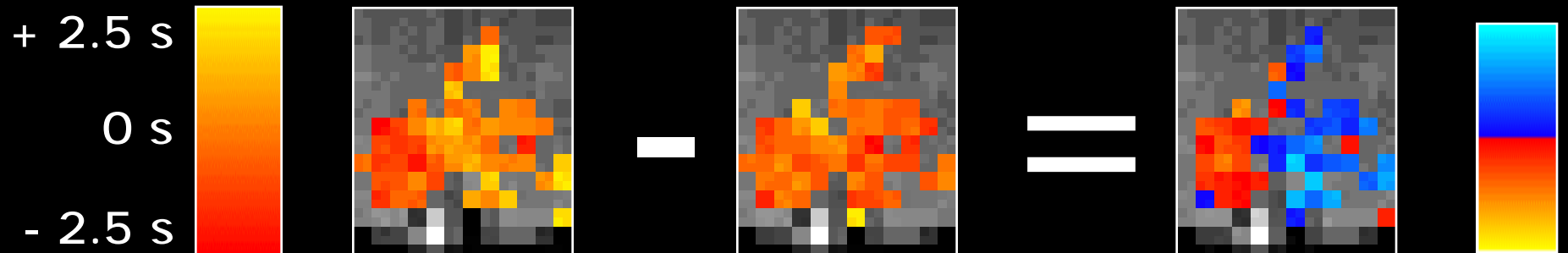


Multi Shot EPI

Excitations	1	2	4	8
Matrix Size	64 x 64	128 x 128	256 x 128	256 x 256
				

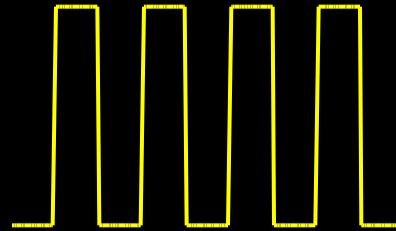


Right Hemifield
Left Hemifield

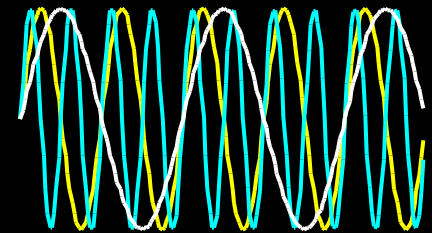


Neuronal Activation Input Strategies

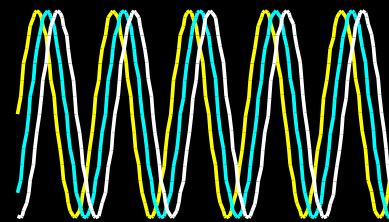
1. Block Design



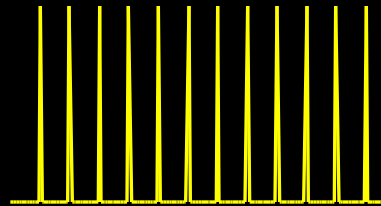
2. Frequency Encoding



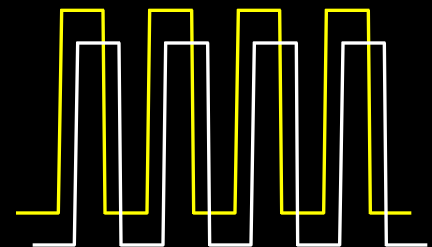
3. Phase Encoding



4. Single Event



5. Orthogonal Block Design



6. Free behavior Design